NACA

RESEARCH MEMORANDUM

FLIGHT DETERMINATION OF DRAG AND PRESSURE RECOVERY OF A NOSE INLET OF PARABOLIC PROFILE AT MACH NUMBERS FROM 0.8 TO 1.7

By Richard I. Sears and C. F. Merlet

Langley Aeronautical Laboratory
Langley Field, Va.

NATIONAL ADVISORY COMMITTEE
FOR AERONAUTICS

WASHINGTON
October 15, 1951

Classification cancelled (or changed to) Unclassified

By authority of NASA Tech Pub Announcement #116
(OFFICER OR CLERK AUTHORIZED TO CHANGE)

5 July 67

By

NK

GRADE OF OFFICER MAKING CHANGE)

31 Mar. 64

DATE

NATIONAL ADVISORY COMMITTEE FOR AERONAUTICS

RESEARCH MEMORANDUM

FLIGHT DETERMINATION OF DRAG AND PRESSURE RECOVERY OF A NOSE INLET OF PARABOLIC PROFILE AT MACH NUMBERS FROM 0.8 TO 1.7

By Richard I. Sears and C. F. Merlet

SUMMARY

A ducted model having a nose inlet whose external contour was defined by a parabolic arc was flight-tested at zero angle of attack. External drag coefficient and total-pressure recovery at the end of the diffuser were measured over a range of Mach numbers from 0.8 to 1.7 and a range of mass-flow ratios from 0.23 to 1.0. The Reynolds number based on the 10-inch body diameter varied from about 4×10^6 to 9×10^6.

At supersonic speeds, the parabolic inlet model had about the same drag coefficient as the basic parabolic body from which it was derived. At low supersonic speeds, the drag of the parabolic inlet was about the same as that of an NACA 1-40-250 nose inlet previously tested. At $M = 1.7$, however, the drag coefficient of the NACA 1-40-250 inlet model was 37 percent greater than that of the parabolic inlet model.

At 0.8 mass-flow ratio, the total-pressure recovery of the present model exceeded that of an external-compression supersonic diffuser at Mach numbers less than 1.4. The reverse was true at higher speeds. The use of a 2.5° diffuser angle eliminated the separation and associated large losses in total-pressure recovery at high mass-flow ratios previously measured for an 8.2° diffuser.

INTRODUCTION

Data pertaining to the drag associated with air inlets at transonic and supersonic speeds are meager relative to that currently available for wings and bodies. In order to investigate the transonic characteristics of air inlets, the Pilotless Aircraft Research Division of the Langley Aeronautical Laboratory is undertaking a series of tests of rocket-propelled models in free flight. The technique involves flying

ducted bodies with various types of air inlets and measuring the total drag, the internal drag, and the total-pressure recovery as functions of Mach number and mass flow.

Data have been obtained in this manner for the NACA 1-40-250 nose inlet and are reported in reference 1. As a continuation of the same program, another nose inlet and diffuser designed to have low drag and good pressure recovery at low supersonic Mach numbers were flight-tested. The results obtained are presented herein. The model was tested at the Langley Pilotless Aircraft Research Station at Wallops Island, Va.

SYMBOLS

C_D	drag coefficient $\left(\frac{D}{\frac{\gamma p_o}{2} M_o^2 A_f}\right)$
m	mass flow through duct
m_o	mass flowing through a stream tube of area equal to inlet area under free-stream conditions
M	Mach number
p	static pressure
H	total pressure
$\overline{H}$	average total pressure
D	drag
A	area
γ	ratio specific heats

Subscripts:

o	free stream
1	first minimum station
f	frontal
i	inlet

MODEL, INSTRUMENTATION, AND TESTS

Model.- A photograph of the nose-inlet model of the present tests is shown in figure 1 and drawings of the model are shown in figure 2. The external shape of the model was derived from that of the parabolic arc body described in reference 1, by simply cutting off the nose portion 5.45 inches aft of the nose to form the inlet. The body coordinates are thus the same as those given in reference 1 and the external contour of the inlet is that generated by a parabolic arc from the inlet station to the station of maximum body diameter. Consequently, the inlet of the present tests is referred to herein as the parabolic nose inlet. The model was stabilized by four 60° half-delta fins of NACA 65A004 airfoil section. The total exposed fin area was 3.7 square feet. This fin configuration is the same as that for the models of reference 1.

The inlet area taken at the most forward station on the model where the diameter was 2.83 inches (fig. 2(b)), was 8 percent of the body frontal area. The inlet lips were made tangent at the leading edge to a circle of 0.012-inch radius. To provide a bellmouth for subsonic operation at very high mass-flow ratios, the duct was contracted to an area 88 percent of the inlet area at a station 0.42 inch aft of the inlet. In an attempt to delay separation evident at high mass-flow ratios in the tests of reference 1, the diffuser for this model was made with a smaller angle. The minimum section was followed by a 2.5° total-angle conical diffuser until the area increased to 1.2 times that of the minimum area. At this station, transition was made to a 3.5° total-angle conical diffuser. The maximum to minimum diffuser area ratio was 2.3, as compared to 2.0 for the diffuser of reference 1. At the end of the diffuser, the duct was contracted to form a throat station. Aft of the throat station, four vane-type shutters were installed to govern the mass flow of air. An electric motor caused these shutters to rotate during flight thereby varying the air flow. The rate of air-flow variation was about 2.2 cycles per second at $M = 1.7$ and increased to about 2.6 cycles per second at $M = 0.8$.

Instrumentation.- At the throat station, static pressure was measured by six wall orifices equally spaced around the circumference of the duct and manifolded together. At the same station, total pressure was measured by three tubes located at 0.00, 0.58, and 0.92 radius from the center line of the duct. Preflight jet tests of reference 1 showed that three tubes would adequately define the total-pressure distribution at this station. Exit static pressure was measured by four inner-wall orifices equally spaced circumferentially 1 inch from the aft end of the model and manifolded together. Total drag was measured by means of a longitudinal accelerometer. A six-channel telemeter was used to transmit a continuous time history of the

five pressure measurements and of the accelerometer reading to ground receiving stations.

Velocity was determined from Doppler radar measurements. Ambient air conditions were determined from radiosonde observations. Altitude was computed from the flight path determined by an NACA modified SCR584 tracking radar.

Tests.- The model was launched at 60° elevation angle and accelerated to maximum speed by a Deacon booster rocket. After burnout of the rocket motor, drag separation of the booster from the model occurred. All data were obtained during the ensuing period of coasting flight during which the model decelerated to subsonic speeds. The angle of attack was essentially zero. The Reynolds number of the test, based on the 10-inch maximum body diameter, is shown in figure 3 as a function of Mach number.

METHOD OF ANALYSIS

The external drag is defined as the dragwise component of the aerodynamic pressure forces and the viscous forces acting on the external contour of the model plus the additive drag. The additive drag is defined as the dragwise component of the aerodynamic pressure forces acting on the exterior of the entering streamline which divides the internal from the external flow.

The external drag was obtained by subtracting the internal drag from the total drag, which was computed from the accelerometer readings. The method of computing the internal drag, the mass-flow ratio, and the total-pressure recovery from the measured pressures is fully explained in reference 1. The maximum value of the internal drag coefficient was about 0.09 and occurred at maximum mass-flow ratio.

The maximum internal air flow is indicated in figure 4 in terms of the ratio of the area of the entering free-stream tube to the inlet area, which ratio is equal to the mass-flow ratio. The test points represent the values of the mass-flow ratio calculated from the measured static and total pressures at the throat station. The solid line represents the maximum mass-flow ratio calculated from one-dimensional flow theory assuming sonic velocity at the first minimum section and, at supersonic speeds, a normal shock ahead of the inlet.

Inasmuch as it is to be expected from the geometry of the model that the maximum mass flow would be limited by choking at the first minimum section, the good agreement between measured and calculated

maximum mass flow lends confidence in the quantities computed from the limited pressure instrumentation possible in this flight model.

Because the inlet choked and the cross-sectional area at the shutter station was large relative to the minimum section, the mass flow remained constant at the maximum value indicated in figure 4 for about one-half of each pressure cycle, that is, for about 0.2 second. During this period of time, the model traveled on the order of 30 to 50 body lengths depending on the Mach number. The flow pattern therefore was that for steady-state flow at the particular Mach number when the mass-flow ratio was a maximum.

At minimum mass flow, the time rate of change of mass flow was also zero and was small for small values of the mass-flow ratio. The conditions at minimum mass flow, therefore, very closely approximate steady-state conditions.

At values of mass flow between the minimum and the maximum, the measured data contained transient terms because of the time rate of change of velocity within the duct. The magnitude of the transient terms did not exceed $\Delta C_D = \pm 0.01$ and $\frac{\Delta H}{H_o} = \pm 0.02$. The method used in reducing these transient components in the measured quantities to negligible values is discussed in reference 1. The data presented, therefore, represent steady-state flow conditions, having been measured under steady-state conditions for the minimum and maximum mass flow ratios and having been reduced to steady-state conditions at intermediate mass-flow ratios.

It is believed that the maximum errors in the absolute magnitude of the data presented are within the following limits:

$\bar{H}/H_o$	± 0.01
M	± 0.005
m/m_o	± 0.02
C_D, at $M = 1.6$	± 0.008
C_D, at $M = 1.2$	± 0.015
C_D, at $M = 0.9$	± 0.030

The accuracy of the changes measured in the drag coefficient as the Mach number and mass-flow ratio varied are believed to be considerably better than the absolute accuracies quoted above.

[redacted]

RESULTS AND DISCUSSION

Drag.- Curves of external drag coefficient for the parabolic inlet model tested are shown in figure 5 as a function of Mach number for several mass-flow ratios. Also shown is the curve of total minus base drag coefficient for the basic body and the external drag coefficient curve for the NACA 1-40-250 nose inlet at $\frac{m}{m_o} = 0.8$ (reference 1), as well as the estimated curve of fin drag coefficient. The drag data for the parabolic inlet model are shown in figure 6 as a function of mass-flow ratio for several Mach numbers.

It is apparent from figure 5 that the drag rise of the parabolic-inlet model starts at a lower Mach number than that for the basic parabolic body. At all Mach numbers, the inlet model has drag coefficients approximately the same as those for the basic body model. The drag coefficient of both models reached a maximum at $M = 1.1$ and decreased as the Mach number increased further.

As indicated in figure 4, the maximum mass-flow ratio varied with Mach number and a mass-flow ratio of 1 was obtained only at $M > 1.65$. The drag-coefficient curve of figure 6 for $M = 1.7$ indicates that the drag varies smoothly with mass-flow ratio right up to $\frac{m}{m_o} = 1.0$. It seems reasonable to expect that if the internal contraction had been eliminated so as to permit a mass-flow ratio of 1 at lower Mach numbers, the drag coefficient would have been that indicated by extrapolation of the curves of figure 6 to $\frac{m}{m_o} = 1$. It is therefore apparent that, by limiting the maximum m/m_o attainable, the internal contraction ratio (0.88) used on this model to provide a bellmouth shape for subsonic operation caused only a slight increment in drag at supersonic speeds over that obtainable with no contraction.

The drag-coefficient increment associated with operation at mass-flow ratios less than 1 is less than that due to the additive drag alone because of the reduction in body pressure drag. This is more clearly shown in figure 7 for $M = 1.4$. The additive drag has been estimated from one-dimensional flow theory assuming the stagnation point at the leading edge of the lips and uniform flow at the inlet. The sum of the pressure and viscous drag of the inlet model is shown in this figure to be less than that of the basic parabolic body at all mass-flow ratios.

The present nose inlet was derived by cutting off the forward 5.45 inches of the parabolic body of reference 1. If the same body is cut off at other stations, a family of inlets can be formed, each having a different inlet area. The drag of these other inlet configurations can be estimated by generalizing the results already obtained as shown

in figure 8. Here the drag coefficients for various inlet-body-fin combinations are plotted as a function of the inlet station, measured from the apex of the basic body. The data are presented for $M = 1.4$ and $\frac{m}{m_o} = 1.0$. The curve is defined by three points. The point at $\frac{X}{d} = 0$ is that for the basic parabolic body (reference 1) and represents the limiting case as the inlet size is decreased. The middle point on the curve was obtained from the present test results by extrapolating the C_D curve (fig. 6) from m/m_o of 0.95 to 1.0. The point at $\frac{X}{d} = 3.6$ represents an inlet whose area is equal to the body frontal area. The forebody is of zero length and hence the forebody C_D is zero. The afterbody drag coefficient was approximated by subtracting from the measured drag coefficient for the basic body the computed pressure and viscous drag of the portion of the body ahead of the maximum diameter. The pressure drag was computed from linear theory (reference 2) and the viscous drag was estimated on the basis of wetted area by using a friction drag coefficient from compressible turbulent-boundary-layer theory (reference 3).

This method of approximating the afterbody drag results in the assumption of a small suction pressure rather than free-stream pressure at the forward end of the afterbody. The correct afterbody drag should be less than that indicated on figure 8 by some small amount. The approximation is thus conservative for the purposes for which the afterbody drag is used in figure 8.

For an airplane, the exit area necessary to permit passage of the air flow required by the turbojet engine may in some cases be somewhat larger than that of the test model, and the afterbody drag should be computed accordingly. Calculations indicate, however, that, if the aft end of the body is cut off farther forward so that the ratio of exit to frontal area is increased from 0.20 to 0.40, the afterbody C_D is decreased by only about 0.006.

The data of figure 8 have been faired with a rather broad band to indicate that the values of C_D are not precisely defined by the data available. The curve indicates a trend of decreasing drag coefficient at maximum mass flow as the inlet area is increased.

The present inlet is compared with the NACA 1-40-250 inlet (reference 1) in figure 5. The nose-inlet configuration of reference 1 had a larger inlet area, lesser fineness ratio, and blunter profile than the inlet of the present test. At subsonic speeds, the differences in drag coefficient of the models may not be significant because of the inability of the accelerometers used to measure accurately small decelerations. The drag-rise Mach number is significant, however, and was about 0.03 lower for the parabolic inlet. The two inlet models, at 0.8 mass-flow ratio, had about the same drag coefficient at low supersonic Mach numbers.

As the Mach number increased further, the drag-coefficient curve of the two models diverged. At a Mach number of 1.7, the drag coefficient of the NACA 1-40-250 inlet model was 37 percent greater than that of the parabolic inlet model.

Total-pressure ratio.- The values of total-pressure recovery were weighted on the basis of area rather than on mass flow. A check for several cases with the most nonuniform distribution of total pressure encountered indicated the mass flow weighted average to be higher than the area weighted average by about $\frac{\Delta\bar{H}}{H_o} = 0.002$, a value well within the experimental accuracy.

Values of the average total-pressure-recovery ratio measured at the end of the diffuser are shown in figure 9 as a function of Mach number and in figure 10 as a function of mass-flow ratio. For $\frac{m}{m_o} < 0.4$ at all supersonic Mach numbers, the recovery was equal to that behind a normal shock, any subsonic diffuser loss being within the accuracy of the measurements.

Large total-pressure losses were reported in reference 1 for an 8.2° total angle diffuser. In an effort to alleviate apparent flow separation, the initial diffusion angle was reduced to 2.5° for the present model. The contraction ratio from the inlet to the first minimum was 1 percent greater for the present model than for that of reference 1. The ratios of the average total pressure measured after diffusion to that at the first minimum station are plotted in figure 11 for the two diffusers as a function of the Mach number at the first minimum station. Conditions at the first minimum station were computed from one-dimensional flow theory and therefore represent average quantities. The subsonic diffuser performance, when presented in this manner, is seen to be independent of the free-stream Mach number in the range tested. The scatter of the points is of about the same magnitude as the inaccuracies in the measurements. Comparison of the pressure-recovery data for the two diffusers indicates that the small angle diffuser did eliminate the severe separation at high mass-flow ratios.

The total-pressure recovery at the end of the diffuser has been computed by using the calculated curves of reference 4 and a skin-friction coefficient of 0.003. For the condition of sonic velocity at the first minimum section, the total pressure after diffusion is computed to be 0.985 times that at the minimum section for the present configuration. The measured value was 0.98, indicating the losses are probably entirely due to skin friction. The corresponding computed recovery for the 8.2° diffuser of reference 1 is 0.995, but the experimental data showed much greater losses, indicating the presence of separation.

The dashed-line curves of figure 9 show the pressure recoveries reported in reference 5 for an external-compression supersonic inlet (Ferri type, 30° cone). At 0.8 mass-flow ratio, the pressure recoveries of the present inlet-diffuser combination exceed those for the supersonic diffuser at Mach numbers less than 1.4. At Mach numbers higher than 1.4 the external-compression diffuser was superior from the standpoint of pressure recovery.

CONCLUSIONS

Flight-test results for a parabolic nose-inlet model and comparison of these with other data indicate the following:

1. At all speeds tested the drag coefficient of the parabolic nose-inlet model was about the same as that of the basic parabolic body from which the inlet model was derived. At a Mach number of 1.1, the drag coefficient of both models reached a maximum and decreased as the Mach number increased further.

2. The parabolic nose inlet and the NACA 1-40-250 nose inlet models had about the same drag coefficient at low supersonic Mach numbers. As the Mach number increased further the drag-coefficient curves of the two models diverged. At a Mach number of 1.7, the NACA 1-40-250 inlet model had about 37 percent greater drag than the parabolic-inlet model.

3. The drag coefficient increment associated with operation at mass-flow ratios less than one was less than that due to the additive drag alone because of a reduction in body pressure drag. The use of an internal contraction ratio of 0.88 at the inlet to provide a bell-mouth for subsonic operation was therefore not accompanied by severe drag penalties.

4. At 0.8 mass-flow ratio, the total-pressure recovery at the end of the diffuser exceeded that of an external-compression supersonic diffuser up to a Mach number of 1.4. At higher Mach numbers the external-compression diffuser was superior.

5. Use of an initial diffuser angle of 2.5° eliminated the separation and consequent large total-pressure losses at high mass-flow ratios previously measured for an 8.2° diffuser.

Langley Aeronautical Laboratory
National Advisory Committee for Aeronautics
Langley Field, Va.

REFERENCES

1. Sears, Richard I., and Merlet, C. F.: Flight Determination of the Drag and Pressure Recovery of an NACA 1-40-250 Nose Inlet at Mach Numbers from 0.9 to 1.8. NACA RM L50L18, 1951.

2. Von Kármán, Theodor, and Moore, Norton B.: Resistance of Slender Bodies Moving with Supersonic Velocities with Special Reference to Projectiles. Trans. A.S.M.E., vol. 54, no. 23, Dec. 15, 1932, pp. 303-310.

3. Van Driest, E. R.: Turbulent Boundary Layer in Compressible Fluids. Jour. Aero. Sci., vol. 18, no. 3, March 1951, pp. 145-160, 216.

4. Beeton, A. B. P.: Curves for the Theoretical Skin Friction Loss in Air Intake Ducts. TN No. Aero 2035, British R.A.E., Feb. 1950.

5. Ferri, Antonio, and Nucci, Louis M.: Preliminary Investigation of a New Type of Supersonic Inlet. NACA TN 2286, 1951.

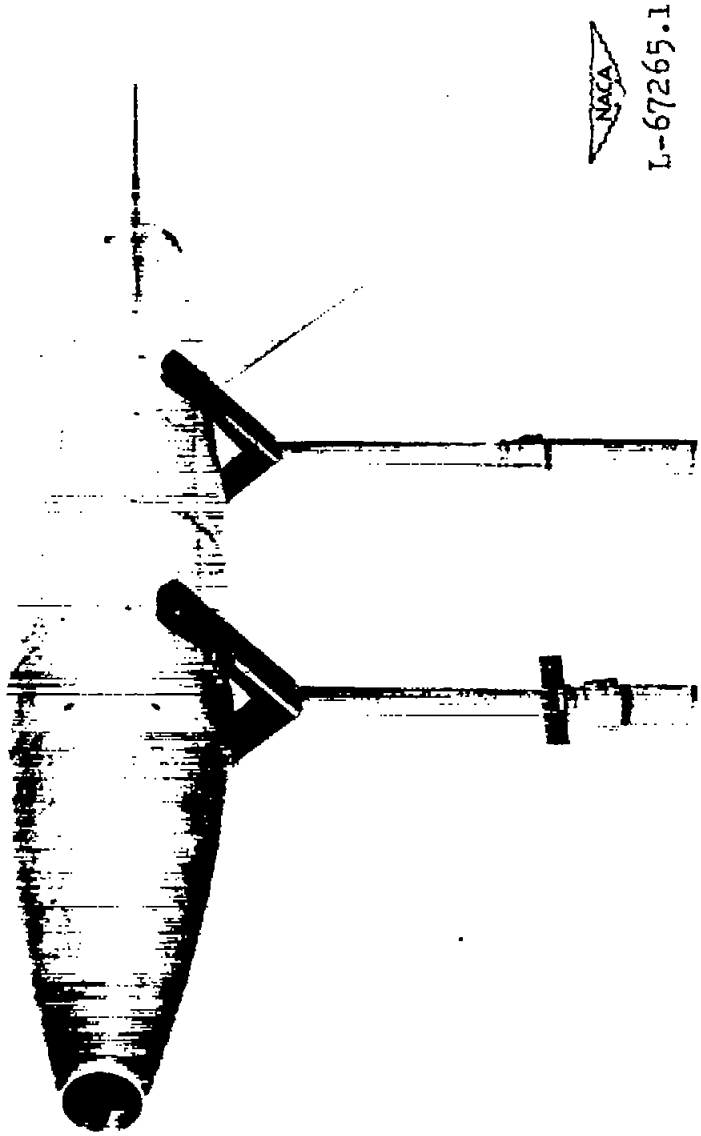

Figure 1.- Photograph of the model.

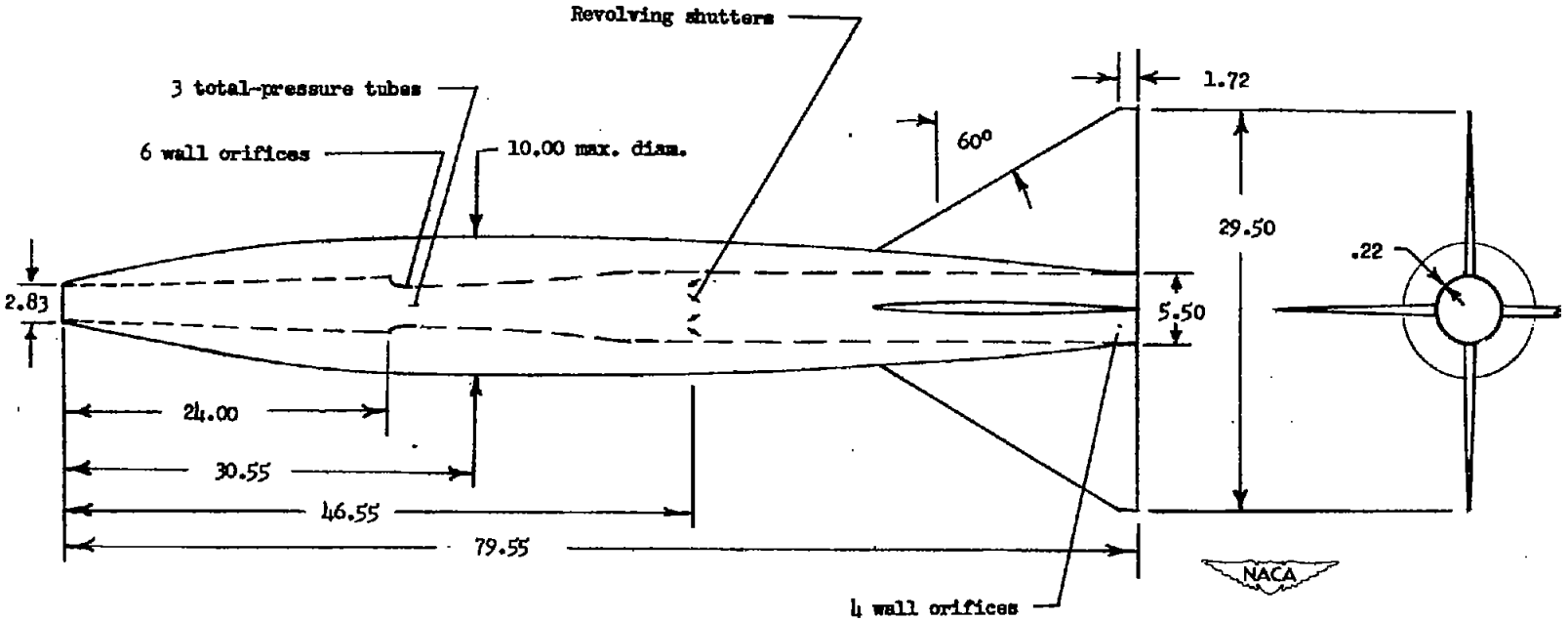

(a) General arrangement.

Figure 2.- Drawings of the model. All dimensions are in inches.

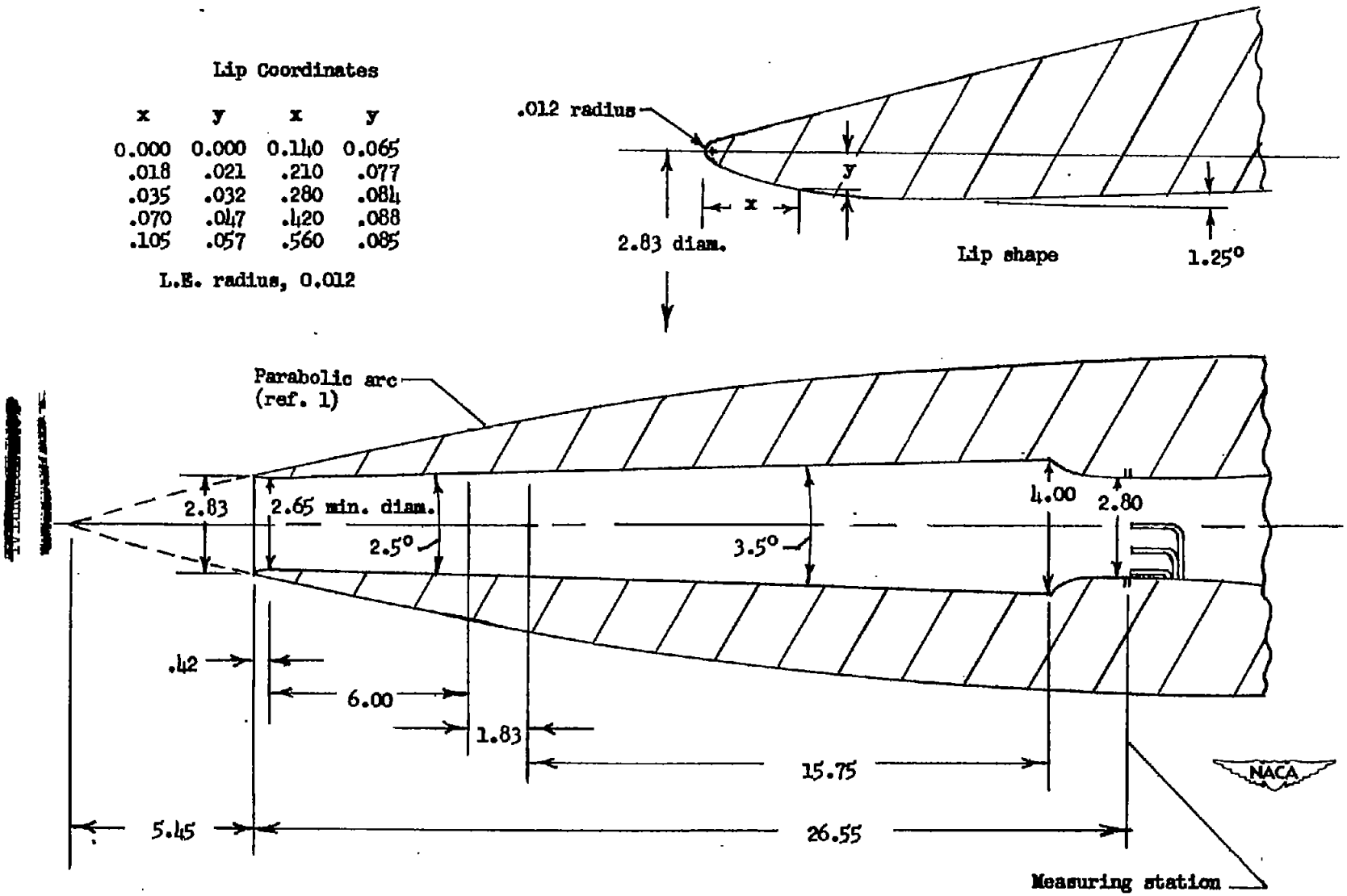

(b) Details of the inlet and diffuser.

Figure 2.- Concluded.

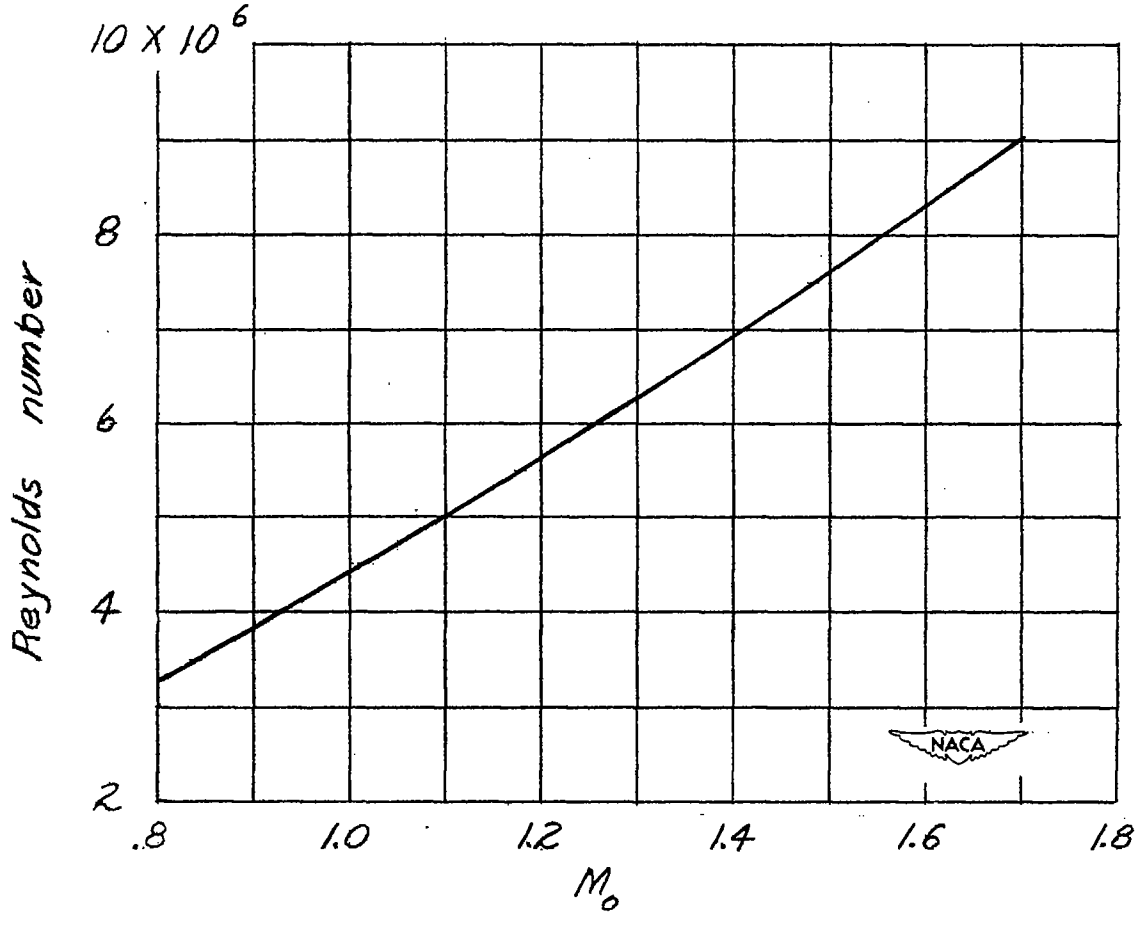

Figure 3.- Variation of Reynolds number with Mach number. Reynolds numbers are based on maximum body diameter of 10 inches.

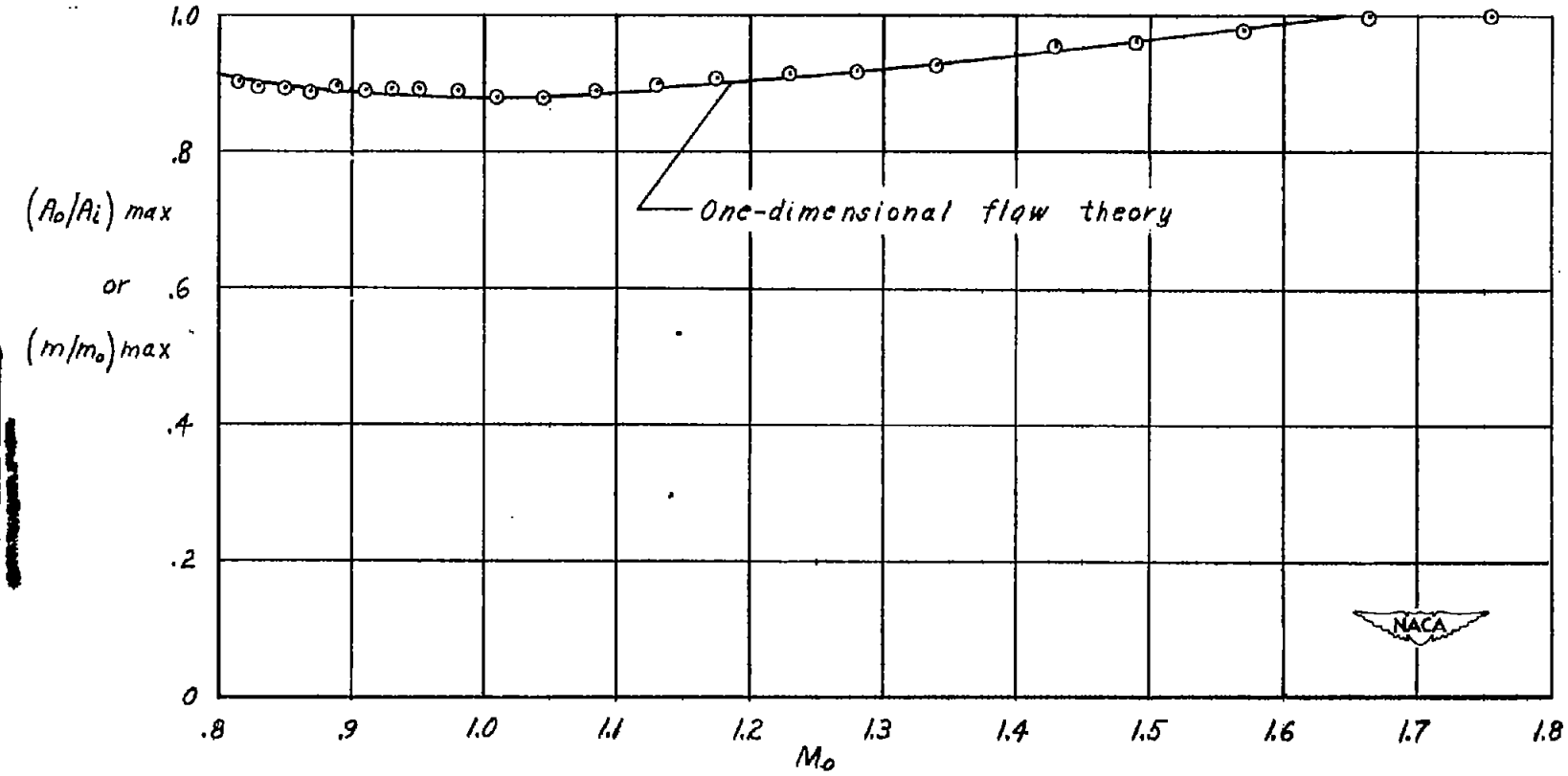

Figure 4.- Measured and computed values of the maximum mass-flow ratio.

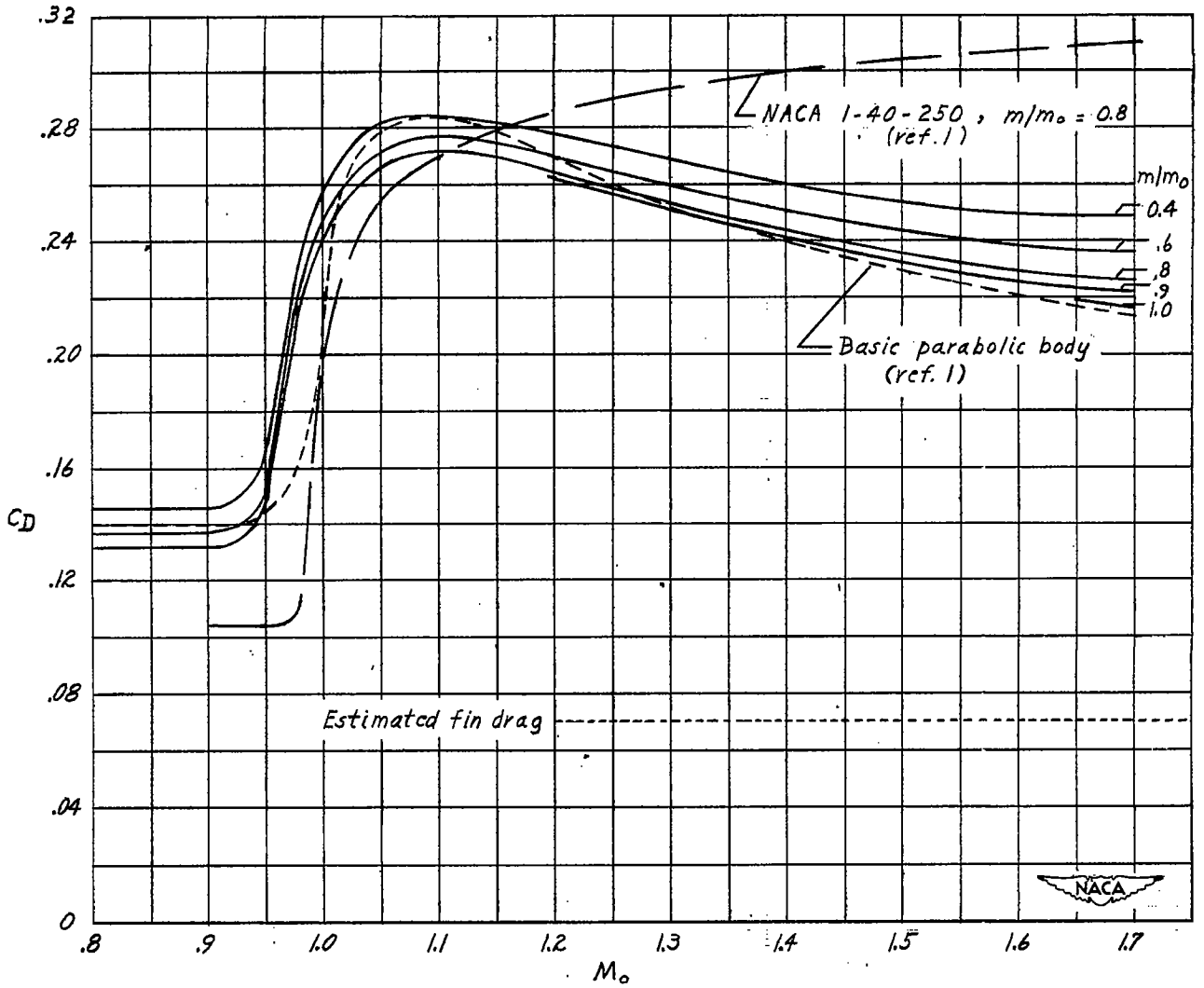

Figure 5.- Variation of external drag coefficient with Mach number for various mass-flow ratios.

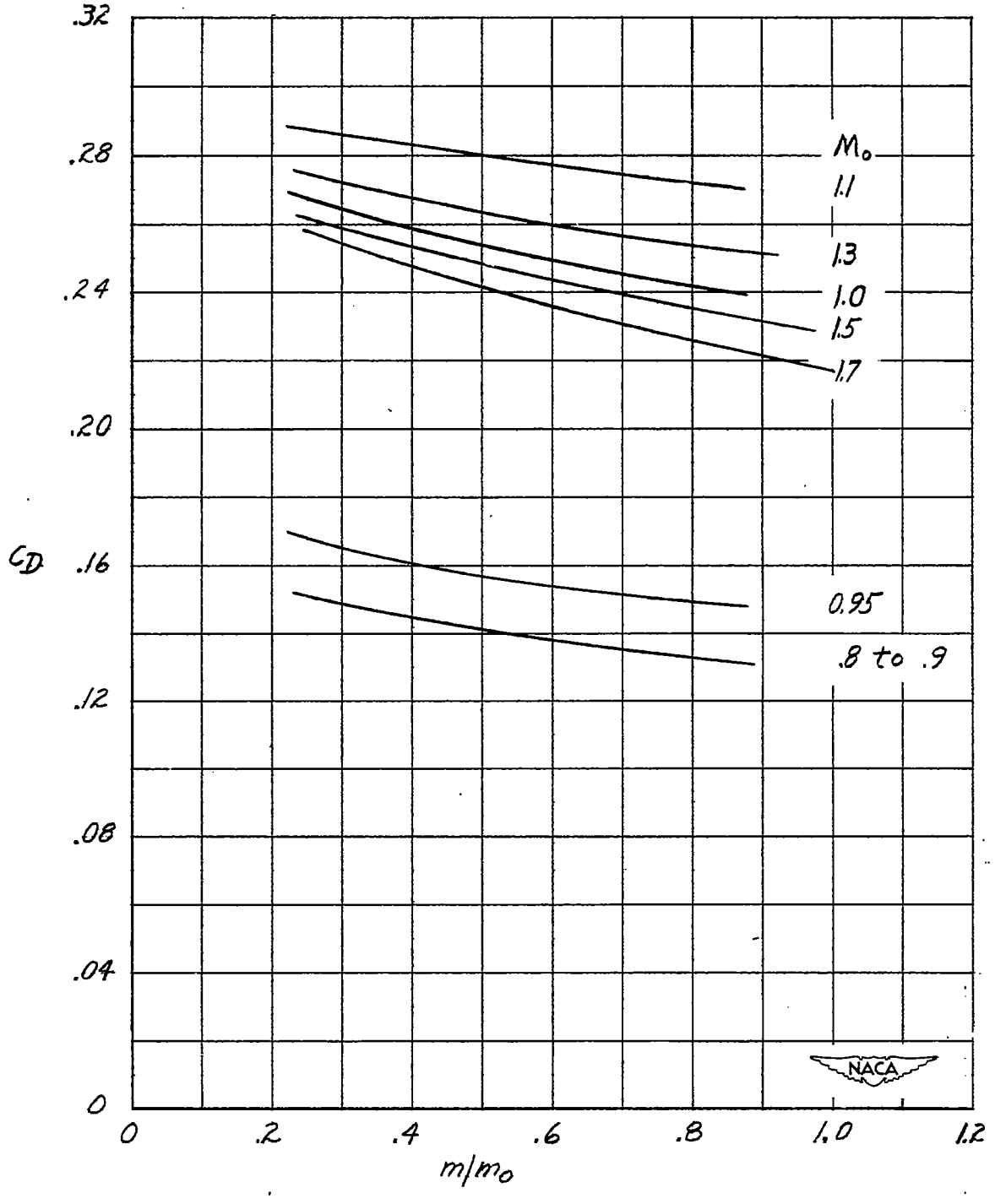

Figure 6.- Variation of external drag coefficient with mass-flow ratio for several Mach numbers.

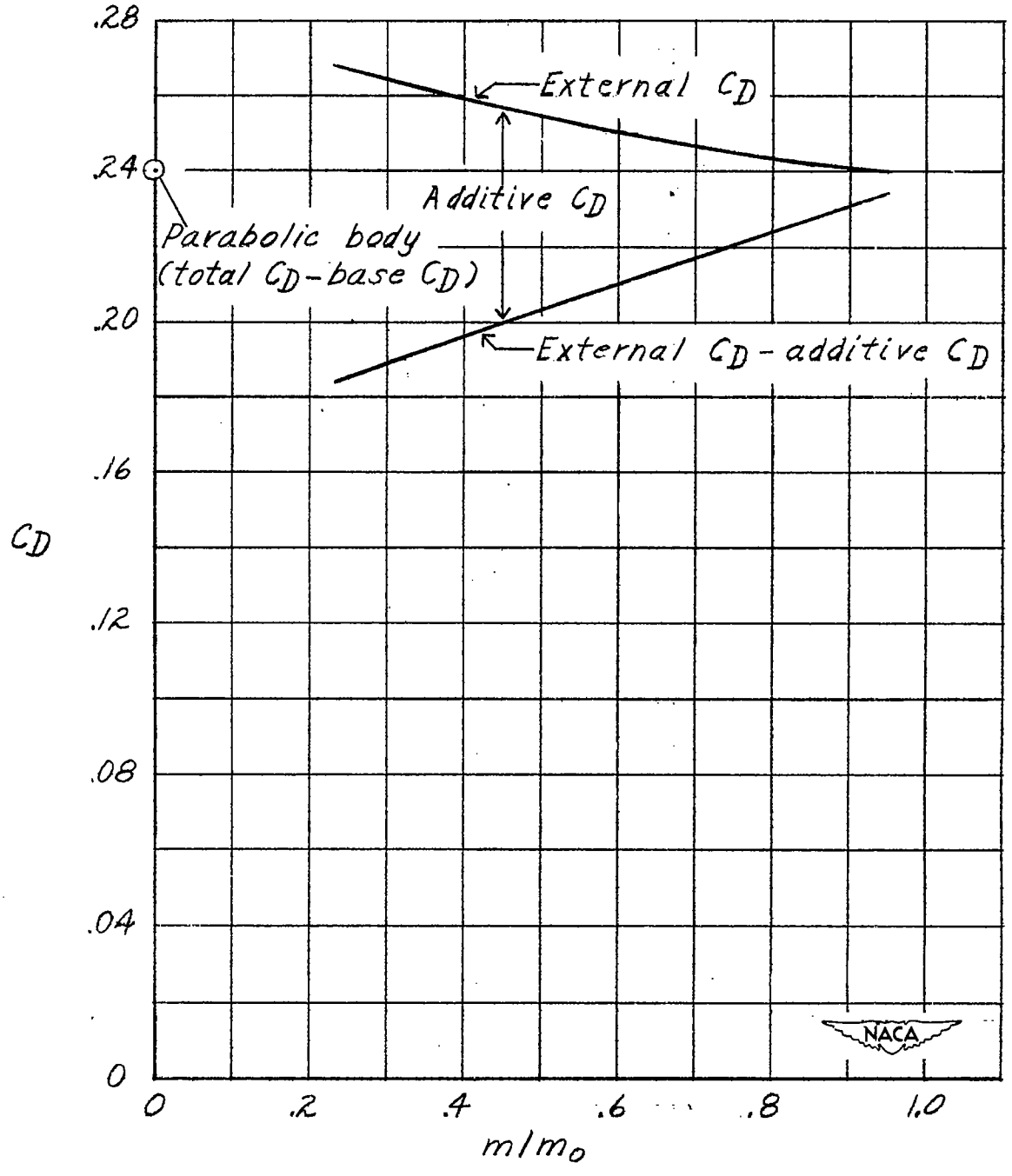

Figure 7.- Measured external and computed additive drag coefficients at a Mach number of 1.4.

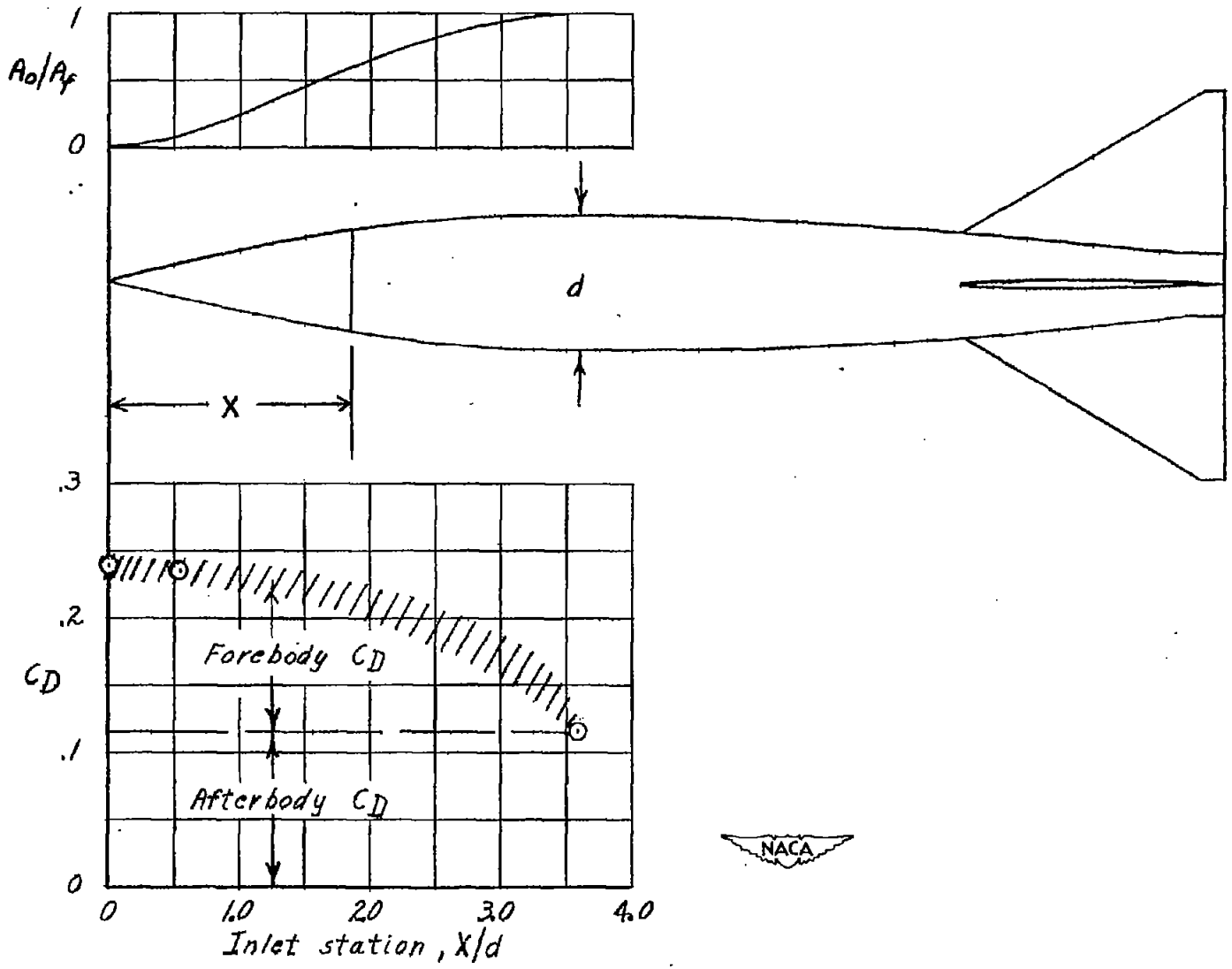

Figure 8.- External drag coefficient for a family of parabolic inlets, $\frac{m}{m_o} = 1.0$; $M_o = 1.4$.

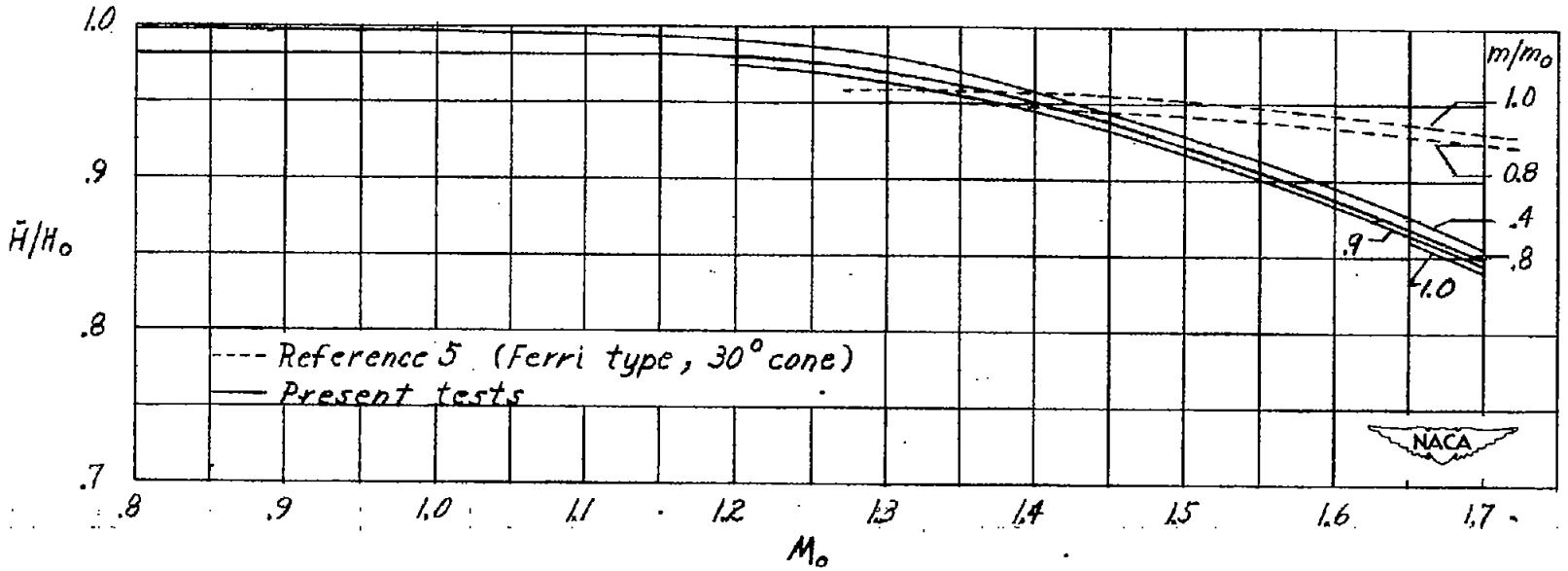

Figure 9.- Variation of total-pressure recovery with Mach number for several mass-flow ratios.

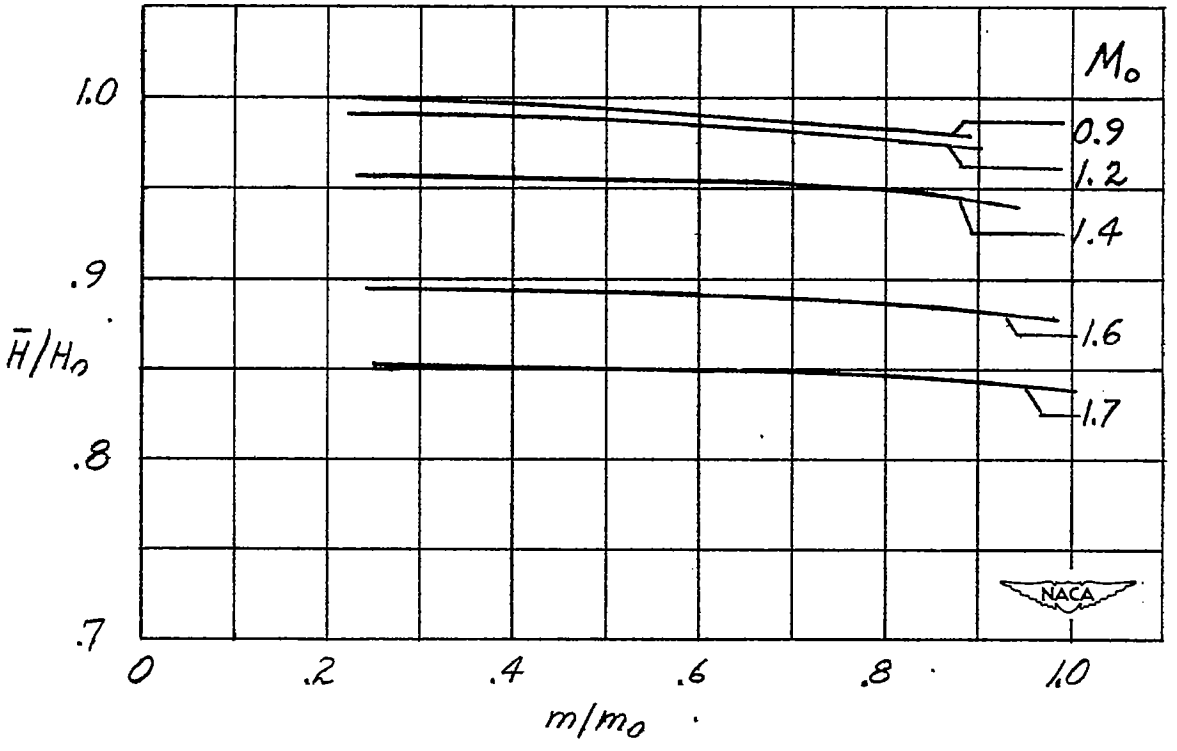

Figure 10.- Variation of total-pressure recovery with mass-flow ratio at several Mach numbers.

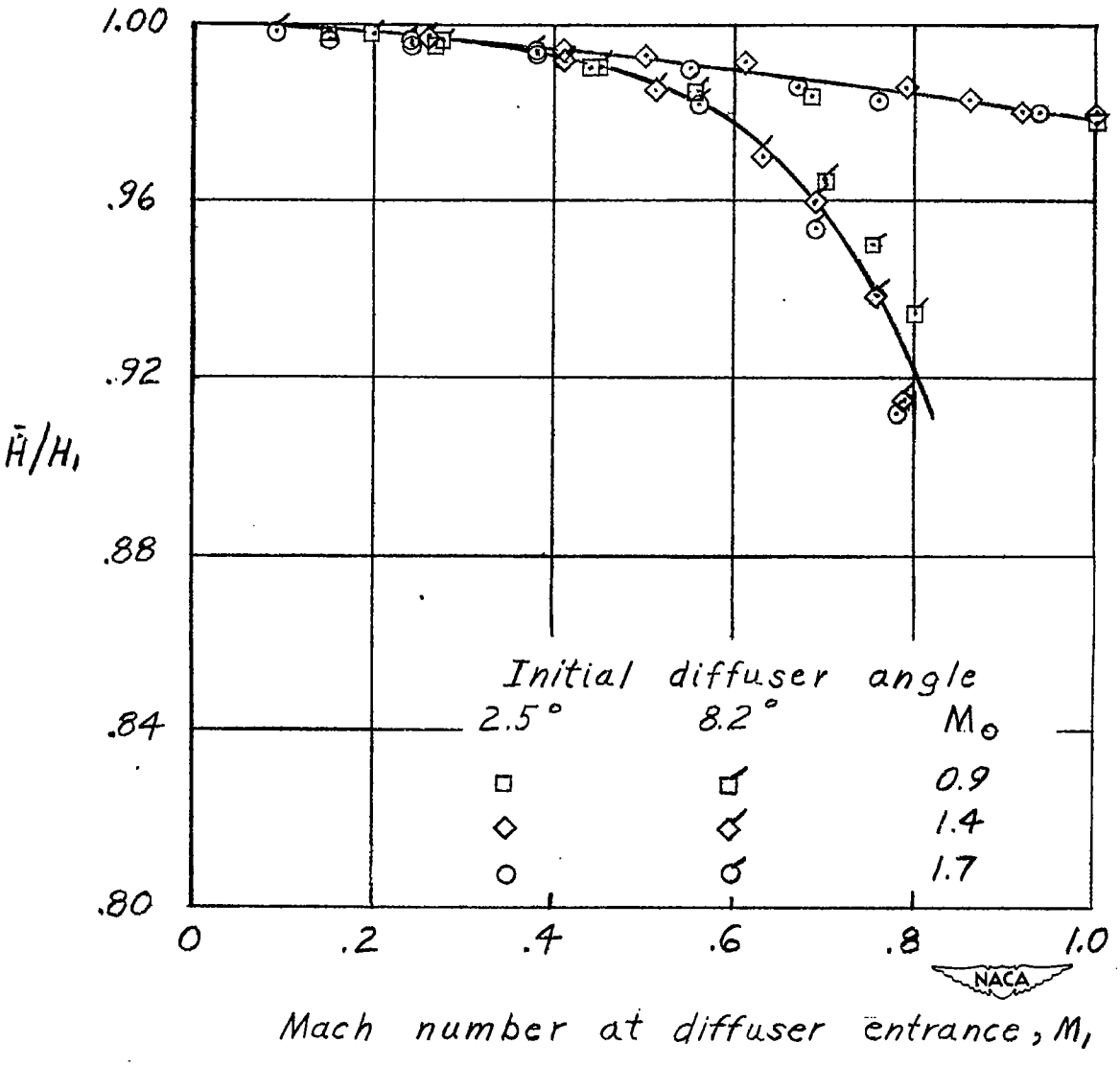

Figure 11.- Comparison at several free-stream Mach numbers of the performance of the 8.2° subsonic diffuser of reference 1 with that for the 2.5° diffuser of the present tests.